EUV and VUV Spectra of NeIII-NeX Line Emissions Observed in the Impurity Gas-Puffing Experiments of the Large Helical Device[*]

Tetsutarou OISHI[1,2], Shigeru MORITA[1,2], Masahiro KOBAYASHI[1,2], Kiyofumi MUKAI[1,2],
Gakushi KAWAMURA[1,2], Suguru MASUZAKI[1,2], Yuki HAYASHI[1], Chihiro SUZUKI[1,2],
Yasuko KAWAMOTO[1], Motoshi GOTO[1,2] and the LHD Experiment Group[1]

[1]*National Institute for Fusion Science, National Institutes of Natural Sciences, 322-6 Toki, Gifu 509-5292, Japan*
[2]*The Graduate University for Advanced Studies, SOKENDAI, 322-6 Toki, Gifu 509-5292, Japan*

Extreme ultraviolet (EUV) and vacuum ultraviolet (VUV) wavelength spectra including line emissions released from neon (Ne) ions ranging from low to high charge states observed simultaneously in a single discharge are summarized for contribution to compile a fundamental spectral dataset for the Ne-seeded divertor heat load reduction experiments in Large Helical Device (LHD). NeIX and NeX lines were observed in the EUV wavelength range of 10~50 Å and NeIII-NeVIII lines were observed in the VUV wavelength range of 400~1000 Å. The temporal evolutions of the line intensities exhibited different behaviors between the edge emissions of NeIII-NeVIII with the ionization potential, E_i, of 63~239 eV and the core emission of NeX with E_i of 1362 eV. NeIX with E_i of 1196 eV exhibited a marginal behavior between the edge emission and the core emission.

1. Introduction

Mitigation of divertor heat load is one of the most critical issues for ITER and future fusion reactors [1, 2]. Enhancement of impurity radiation loss in the edge and divertor plasmas has been widely used to reduce the heat load, which is so called "divertor detachment" operation. In Large Helical Device (LHD), several operational scenarios, such as impurity seeding [3–7] or imposing resonant magnetic fields [8–10], have been proposed and applied to realize and sustain the divertor detachment. In the cases with using gas-puffing for the impurity seeding, nitrogen (N) and noble gases such as neon (Ne), argon (Ar), krypton (Kr), or xenon (Xe) are popular candidates. When impurity ions are introduced into the plasmas, some of them are distributed in the edge plasmas with lower ionization states while others are distributed in the core plasmas with higher ionization states. Impurity ions in the edge plasmas have potential to contribute sustainment of the detached divertor with playing a role of radiators, while those in the core plasma may cause plasma dilution leading to deterioration of the plasma confinement. Therefore, it is important to monitor both the edge impurity in the lower charge states and the core impurity in the higher charge states simultaneously to establish both an effective divertor

detachment and a good core confinement. In some previous studies of Ne seeding experiments, NeII~NeVIII emission lines have been observed as indicators of the edge Ne radiation [11, 12] while NeX emission line has been observed as an indicator of the core Ne radiation [13]. In the present study, extreme ultraviolet (EUV) and vacuum ultraviolet (VUV) spectroscopy diagnostics are applied to measure wavelength spectra including line emissions released from Ne ions ranging from low to high charge states simultaneously in a single discharge of the Ne-seeded divertor heat load reduction experiments in LHD. Observed spectral lines are summarized for contribution to compile a fundamental spectral dataset which are useful for further advanced spectroscopic diagnostics.

2. Experimental Setup

LHD is a heliotron type plasma confinement device which has the major/minor radii of 3.6/0.64 m in the standard magnetic configuration with maximum plasma volume of 30 m^3 and toroidal magnetic field of 3 T [14]. The coil system consists of a set of two continuous superconducting helical coils with poloidal pitch number of 2 and toroidal pitch number of 10, and also three pairs of superconducting poloidal coils. Figure 1 illustrates a schematic drawing of the spectroscopy system using two flat-field grazing incidence EUV spectrometers (EUV Long [15] and EUV Short [16]) and three 20 cm
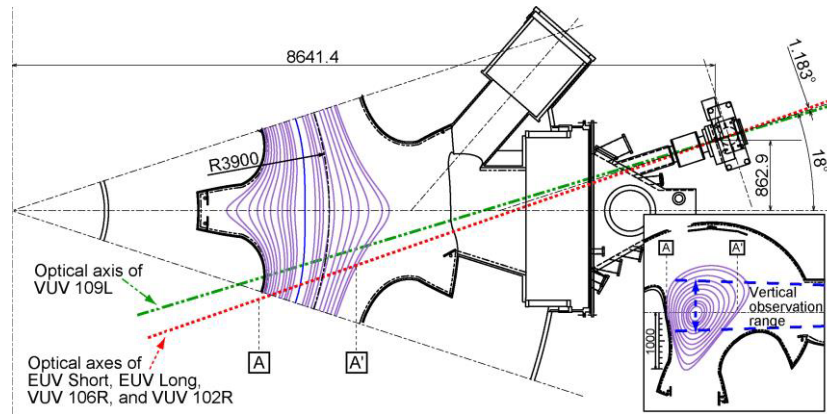
Fig. 1 Schematic drawing of the spectroscopy system using two flat-field grazing incidence EUV spectrometers (EUV Long and EUV Short) and three 20 cm normal incidence VUV spectrometers (VUV 109L, VUV 106R, and VUV 102R) in LHD. Top view of magnetic surfaces ($R_{ax} = 3.6$ m), optical axes of five spectrometers, and the vertical observation range on a plasma cross section including optical axes of the spectrometers shown together.

normal incidence VUV spectrometers (VUV 109L, VUV 106R, and VUV 102R) in LHD [17]. Top view of magnetic surfaces with the position of the magnetic axis, R_{ax}, of 3.6 m, optical axes of five spectrometers, and the vertical observation range on a plasma cross section including optical axes of the spectrometers are shown together. In the Ne gas-puffing experiments described in the next chapter, wavelength ranges of 5~60 Å , 100~300 Å, 300~1050 Å, 970~1870 Å, and 1510~2400 Å were covered by the spectrometers of EUV Short, EUV Long, VUV 109L, VUV106R, and VUV102R, respectively. Back-illuminated CCD detectors (Andor model DO420-BN: 1024×256 pixels, pixel size 26×26 μm^2) were placed at the positions of the exit slits of the spectrometers. A time resolution of 5 ms was applied to measure temporal evolution of the spectra. In this paper, a unit of CCD counts was directly used for signal intensity without absolute calibration. However, we have already established calibration method by using bremsstrahlung emission intensity and its wavelength dependence [18], so we will be able to use the calibrated intensity of the signals when we need detailed discussion with absolute values.

3. EUV and VUV Spectra of Ne Line Emissions

Figure 2 shows a typical waveform of Ne gas injection experiment in LHD with R_{ax} of 3.6 m and the toroidal magnetic field, B_t, of 2.75 T in the counter-clockwise direction from the top view. In this figure, temporal evolution of (a) heating power of the electron cyclotron heating (ECH) and the negative hydrogen ion source-based neutral beam injection (n-NBI), and gas-puffing duration of Ne and H$_2$, (b) central electron temperature, T_{e0}, and line-averaged electron density, $\bar{n}_e$, (c) edge electron temperature, $T_e(a_{99})$, and edge electron density, $n_e(a_{99})$, (d) plasma stored energy, W_p, and total radiation power, P_{rad}, and (e)

toloidally-averaged divertor heat flux, $\langle q_{div} \rangle$, are plotted together. The plasma edge a_{99} was defined as the effective minor radius in which 99% of electron stored energy was enclosed [19]. The plasma was initiated by ECH and further heated by n-NBI. H$_2$ gas was puffed from 3.30 to 5.30 s to control the electron density. Reduction of the divertor heat load was aimed by puffing Ne gas from 4.10 to 4.18 s. After the Ne gas puffing, T_{e0} did not change significantly while $T_e(a_{99})$ decreased drastically. $\bar{n}_e$, $n_e(a_{99})$, and P_{rad} increased rapidly. W_p also increased gradually, which suggested that the Ne injection had no negative effects for the plasma confinement. As an indicator of the divertor heat load, $\langle q_{div} \rangle$ measured by the Langmuir probes mounted on the divertor plates was employed [5]. The $\langle q_{div} \rangle$ value decreased suddenly at 4.18 s and the reduced heat flux was sustained from 4.22 s to 4.32 s. In this time period, $\langle q_{div} \rangle$ was reduced down to about 30% of the value averaged in the time period from 4.00 s to 4.10 s. Then $\langle q_{div} \rangle$ recovered from 4.40 s and P_{rad} also decreased.

As shown in Figs. 2 (b) and (c), $\bar{n}_e$ and $n_e(a_{99})$ exhibited similar temporal evolution. In LHD, most of the discharges have flat or hollow electron density profiles, thus, $n_e(a_{99})$ has similar value to $\bar{n}_e$. Figure 3 shows the radial profiles of the electron temperature, T_e, and the electron density, $\bar{n}_e$ plotted against the effective minor radius, r_{eff}, normalized by a_{99}. The locations of $r_{eff}/a_{99} = \pm 1$ are the plasma edges. The closed and open circles correspond timings before Ne puff and after Ne puff with the reduced divertor flux, respectively. As shown in the figure, n_e increased drastically outer half of the plasma, namely, $r_{eff}/a_{99} > 0.5$ and $r_{eff}/a_{99} < -0.5$, after Ne injection, which is the reason why $\bar{n}_e$ and $n_e(a_{99})$ exhibited similar temporal evolution.

Figure 4 shows EUV/VUV spectra including line emissions released from Ne ions. The spectral data were averaged over 4.00~4.10 s (blue, before Ne puff), 4.22~4.32 s (red, after Ne puff with reduced divertor flux),
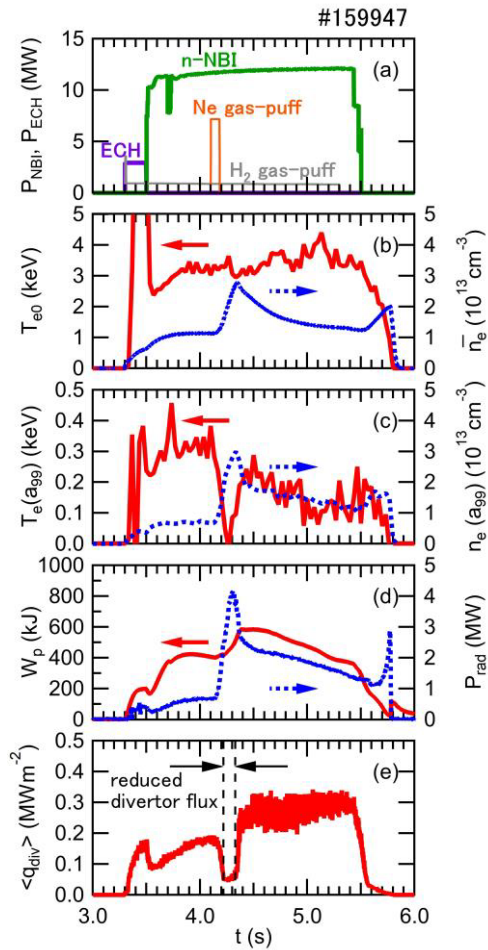
Fig. 2 Typical waveform of Ne gas injection experiment in LHD: (a) heating power of ECH and n-NBI, and gas-puffing duration of Ne and H_2, (b) central electron temperature, T_{e0}, and line-averaged electron density, $\bar{n}_e$, (c) edge electron temperature, $T_e(a_{99})$, and edge electron density, $n_e(a_{99})$, (d) plasma stored energy, W_p, and total radiation power, P_{rad}, and (e) toloidally-averaged divertor heat flux, $\langle q_{div} \rangle$.

Fig. 3 Radial profiles of the electron temperature, T_e, and the electron density, $\bar{n}_e$ plotted against the effective minor radius, reff, normalized by a_{99}. The locations of $r_{eff}/a_{99} = \pm1$ are the plasma edges. The closed and open circles correspond timings before Ne puff and after Ne puff with the reduced divertor flux, respectively.

and 4.40~4.50 s (green, with recovered divertor flux). Identification of Ne line emissions were conducted based on the wavelength database of NIST [20] for NeIII-NeIX lines as well as Ref. [21] for NeX lines. A previous research on detailed line identification of Ne lines in the wavelength range of 250~2300 Å measured using a 3 m normal incidence spectrometer in LHD was also referred [22]. As shown in Fig. 4, strong emissions of NeIX (13.45, 13.55) Å and NeX (10.24, 12.13, 12.14) Å were observed in the wavelength range of 5~60 Å measured by "EUV Short" spectrometer. The wavelength range of 100~300 Å measured by "EUV Long" spectrometer includes relatively strong emissions of NeVI (122.52, 122.70, 122.71) Å, NeVII (106.04, 106.08, 106.09, 106.19, 106.20) Å, and NeVIII (102.91, 103.08) Å as well as many weak emission lines of NeIV-NeVIII. In the wavelength range of 300~1050 Å measured by "VUV 109L" spectrometer,
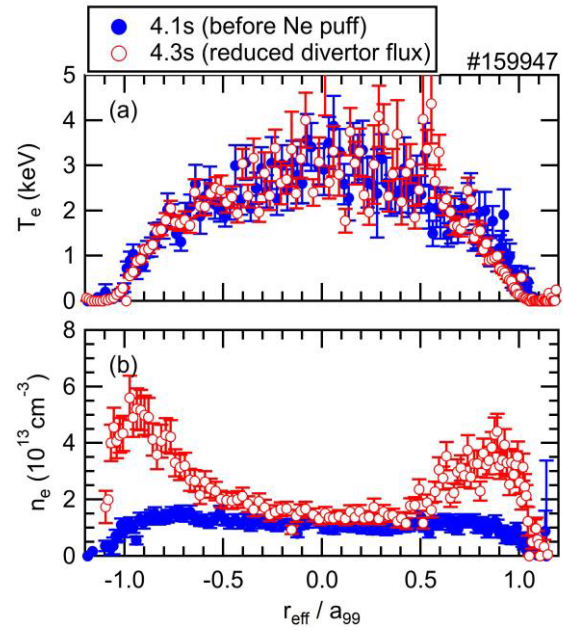
many lines useful for spectroscopy such as NeIII (488.11, 488.88, 489.50, 489.65, 490.31, 491.05) Å, NeIV (541.13, 542.07, 543.88) Å, NeV (481.29, 481.37, 482.99) Å, (568.42, 569.76, 569.83) Å, (572.11, 572.34) Å, NeVI (401.15, 401.94) Å, NeVII 465.22 Å, (561.25, 561.38, 561.73, 562.99, 564.53) Å, and NeVIII 770.41 Å, 780.32 Å were observed. In the wavelength range of 970~1870 Å measured by "VUV 106R" spectrometer, most of the observed lines were higher order emission from lower wavelength ranges. We also acquired spectral data in the wavelength range of 1510~2400 Å measured by "VUV 102R" spectrometer. However, no strong Ne lines were observed in the wavelength range.

Figure 5 shows temporal evolutions of NeIII-NeX emission intensities of which the wavelength spectra were integrated over the wavelength ranges as follows: (a) 487.6~491.0 Å for NeIII (488.11, 488.88, 489.50, 489.65, 490.31, 491.05) Å, (b) 541.6~545.0 Å for NeIV (541.13, 542.07, 543.88) Å, (c) 480.7~484.2 Å for NeV (481.29, 481.37, 482.99) Å, (d) 802.5~805.8 Å for NeVI (401.15, 401.94) × 2 Å, (e) 929.3~932.6 Å for NeVII 465.22 × 2 Å, (f) 778.3~781.6 Å for NeVIII 780.32 Å, (g) 13.39~13.55 Å for NeIX (13.45, 13.55) Å, and (h) 24.17~24.37 Å for NeX (12.13, 12.14) × 2 Å. As shown in the figures, NeIII-NeVIII exhibited similar behavior. Namely, the emissions were enhanced within the time period of the enhanced P_{rad} and reduced $\langle q_{div} \rangle$ after the Ne puff. The values of ionization potential, E_i, of NeIII-NeVIII are less than 300 eV, thus, the emissions are released from the edge plasmas out-
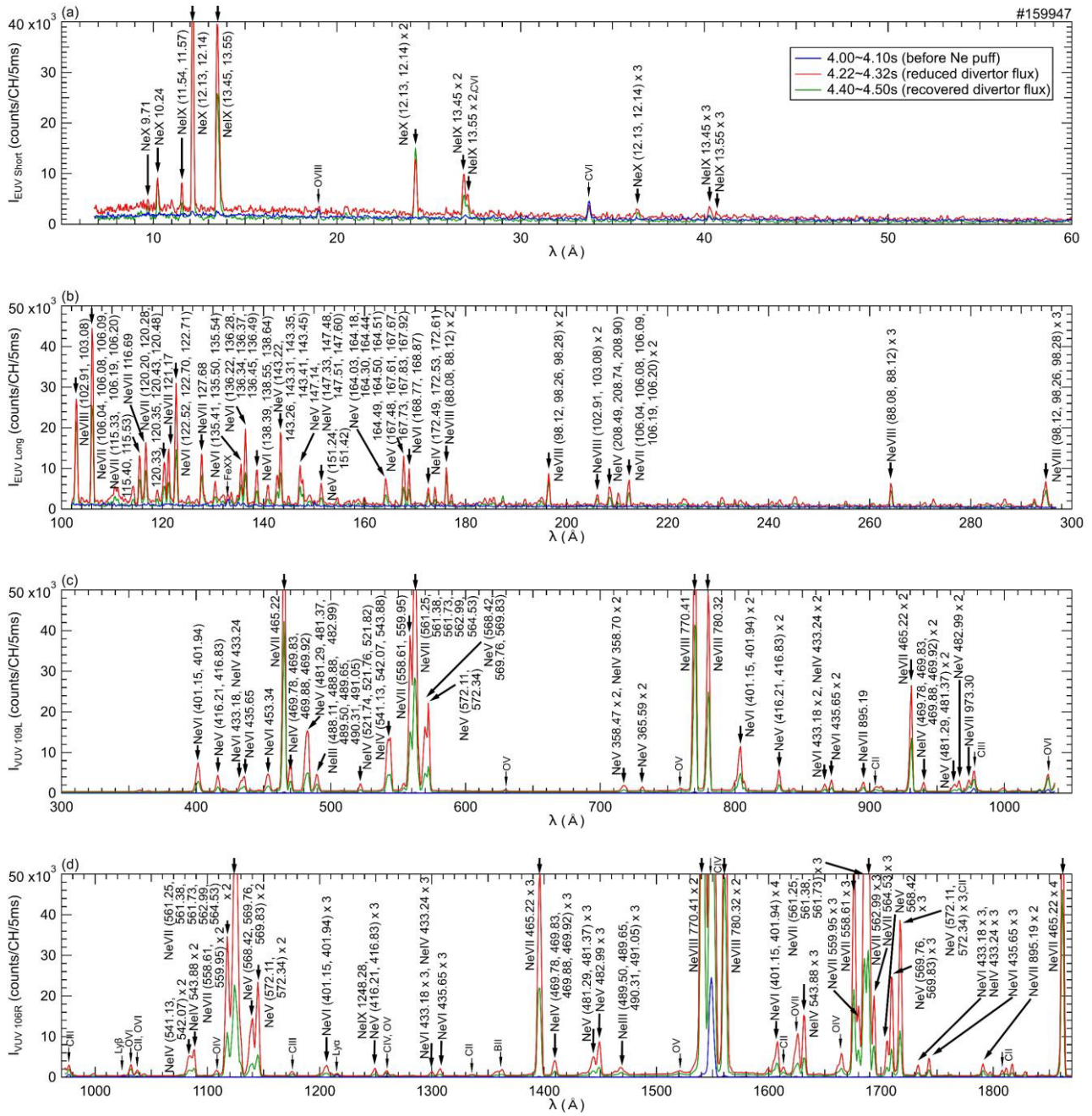
Fig. 4 EUV/VUV spectra including line emissions released from Ne ions in the wavelength range of (a) 5~60 Å measured by "EUV Short" spectrometer, (b) 100~300 Å measured by "EUV Long" spectrometer, (c) 300~1050 Å measured by "VUV 109L" spectrometer, and (d) 970~1870 Å measured by "VUV 106R" spectrometer. The spectral data were averaged over 4.00~4.10 s (blue, before Ne puff), 4.22~4.32 s (red, after Ne puff with reduced divertor flux), and 4.40~4.50 s (green, with recovered divertor flux).

side the last closed flux surface (LCFS). On the other hand, temporal behaviors of NeIX and NeX emissions, which are considered to be released from the confinement region within LCFS because of the larger E_i values of 1196 eV and 1362 eV, respectively, were different from those of the other lower charge states. Figure 6 shows the temporal evolutions of (a) NeVIII, (b) NeIX, and (c) NeX intensities enlarged in the time range of 4.1~4.8 s. NeVIII and NeX clearly exhibited different behaviors and NeIX had a marginal behavior between NeVIII and NeX. A decay

of the emission intensity of NeIX is slower than that of NeVIII and faster than NeX. The reason for the difference between NeIX and NeX has to be investigated, and we suspected difference in spatial profiles of Ne^{8+} and Ne^{9+} ions. As shown in Fig. 3, electron density close to the plasma edge changed significantly compared to the core region. Ne^{8+} with E_i of 1196 eV should be located outer than Ne^{9+} with E_i of 1362 eV, thus, the significant change of the electron density at the edge region is supposed to have larger effect on NeIX rather than NeX.
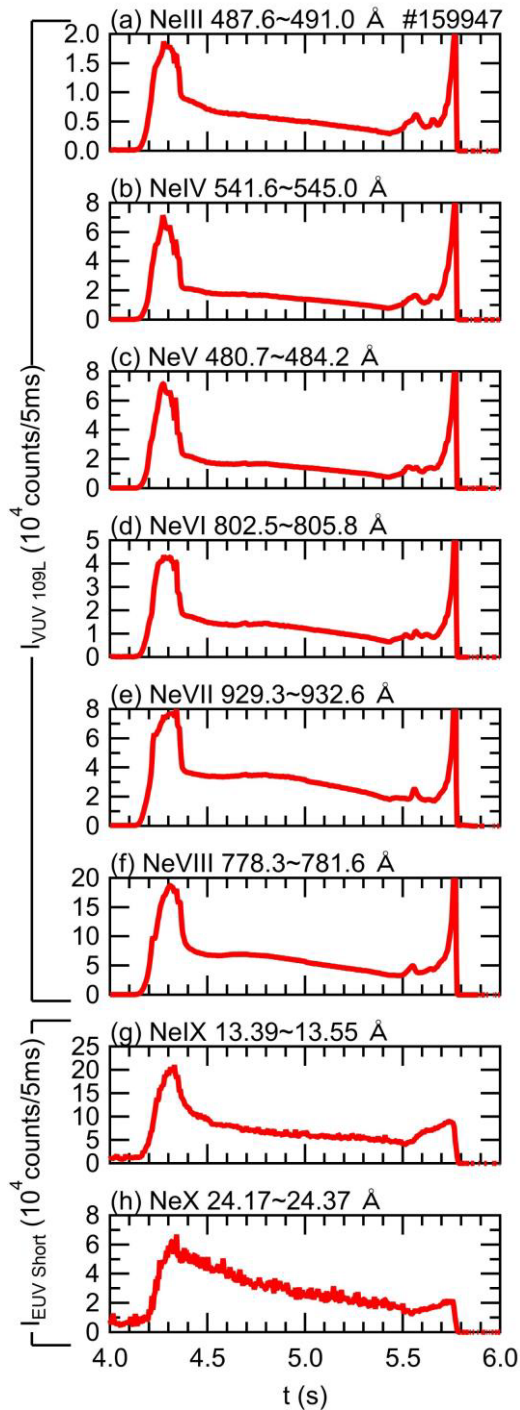
Fig. 5 Temporal evolutions of NeIII-NeX intensities which were integrated over wavelength ranges of (a) 487.6~491.0 Å for NeIII (488.11, 488.88, 489.50, 489.65, 490.31, 491.05) Å, (b) 541.6~545.0 Å for NeIV (541.13, 542.07, 543.88) Å, (c) 480.7~484.2 Å for NeV (481.29, 481.37, 482.99) Å, (d) 802.5~805.8 Å for NeVI (401.15, 401.94)×2 Å, (e) 929.3~932.6 Å for NeVII 465.22×2 Å, (f) 778.3~781.6 Å for NeVIII 780.32 Å, (g) 13.39~13.55 Å for NeIX (13.45, 13.55) Å, and (h) 24.17~24.37 Å for NeX (12.13, 12.14)×2 Å.
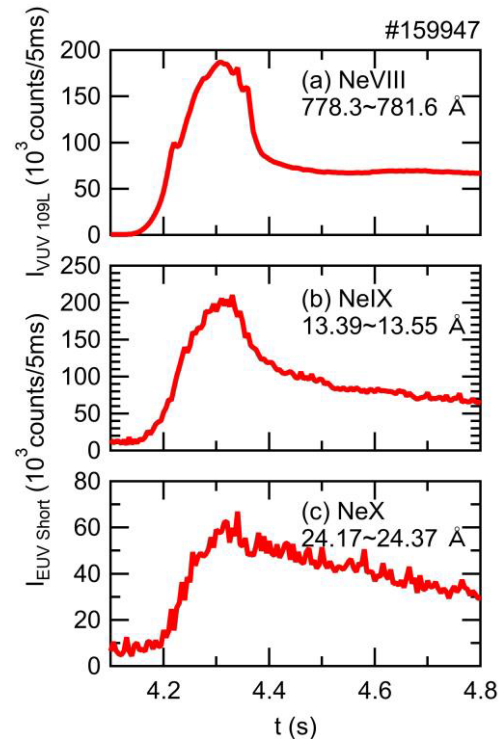

Fig. 6 Temporal evolutions of NeVIII-NeX intensities enlarged in the time range of 4.1~4.8 s. The wavelength ranges were integrated over (a) 778.3~781.6 Å for NeVIII 780.32 Å, (b) 13.39~13.55 Å for NeIX (13.45, 13.55) Å, and (c) 24.17~24.37 Å for NeX (12.13, 12.14)×2 Å.

ify the reason for difference in the temporal evolution of emissions from each charge state. Therefore, it is important for the profile measurements to find and summarize lines which are isolated from other lines in the wavelength and have substantially large intensities. The Ne lines observed in this study are summarized in Table 1 together with E_i for each charge state as useful tools for the further spectroscopic diagnostics. Some of the lines are blended with each other, thus, wavelengths of blended lines are enclosed in parentheses in the table. The lines listed in this table will be used for further spectroscopic researches using space-resolved EUV and VUV spectrometers which have been developed in LHD [23–27]. Comparison between the spectroscopic results and the impurity transport simulation [28] is also planned to reproduce the enhancement of the Ne line emissions coincident with the reduction of the divertor heat load.

4. Summary

The EUV and VUV wavelength spectra including line emissions released from Ne ions ranging from low to high charge states observed simultaneously in a single discharge are summarized for contribution to compile a fundamental spectral dataset for the Ne-seeded divertor heat load reduction experiments in LHD. NeIX and NeX lines were observed in the EUV wavelength range of 10~50 Å and

As stated in the previous paragraph, measurements of spatial profiles of the emission lines are necessary to clar-

Table 1 Useful Ne lines for spectroscopic diagnostics observed in this study. Wavelengths of blended lines are enclosed in parentheses.

Line	E_i (eV)	λ (Å)
NeIII	63	(489.50, 489.65, 490.31, 491.05)
NeIV	97	(541.13, 542.07, 543.88)
NeV	126	(481.29, 481.37, 482.99) (568.42, 569.76, 569.83) (572.11, 572.34)
NeVI	158	(122.52, 122.70, 122.71) (401.15, 401.94)
NeVII	207	(106.04, 106.08, 106.09, 106.19, 106.20) 465.22 (561.25, 561.38, 561.73, 562.99, 564.53)
NeVIII	239	(102.91, 103.08) 770.41 780.32
NeIX	1196	(13.45, 13.55)
NeX	1362	10.24 (12.13, 12.14)

NeIII-NeVIII lines were observed in the VUV wavelength range of 400∼1000 Å. The temporal evolutions of the line intensities exhibited different behaviors between the edge emissions of NeIII-NeVIII with E_i of 63∼239 eV and the core emission of NeX with E_i of 1362 eV. NeIX with E_i of 1196 eV exhibited a marginal behavior between the edge emission and the core emission.

Acknowledgments

[1] ITER Physics Basis, "Chapter 4: Power and particle control", Nucl. Fusion **39**, 2391 (1999).
[2] M. Shimada *et al.*, Nucl. Fusion **47**, S1 (2007).
[3] S. Masuzaki *et al.*, J. Nucl. Mater. **438**, S133 (2013).
[4] K. Mukai *et al.*, Nucl. Fusion **55**, 083016 (2015).
[5] H. Tanaka *et al.*, Nucl. Mater. Energy **12**, 241 (2017).
[6] C. Suzuki *et al.*, Nucl. Mater. Energy **14**, 195 (2019).
[7] K. Mukai *et al.*, Plasma Fusion Res. **15**, 1402051 (2020).
[8] H.M. Zhang *et al.*, Plasma Fusion Res. **11**, 2402019 (2016).
[9] H.M. Zhang *et al.*, Phys. Plasmas **24**, 022510 (2017).
[10] M. Kobayashi *et al.*, Nucl. Fusion **59**, 096009 (2019).
[11] T. Nakano *et al.*, J. Nucl. Mater. **438**, S291 (2013).
[12] C. Suzuki *et al.*, J. Nucl. Mater. **463**, 561 (2015).
[13] G.S. Xu *et al.*, Nucl. Fusion **60**, 086001 (2020).
[14] Y. Takeiri *et al.*, Nucl. Fusion **57**, 102023 (2017).
[15] M.B. Chowdhuri *et al.*, Appl. Opt. **47**, 135 (2008).
[16] M.B. Chowdhuri *et al.*, Rev. Sci. Instrum. **78**, 023501 (2007).
[17] T. Oishi *et al.*, Plasma Fusion Res. **10**, 3402031 (2015).
[18] C.F. Dong *et al.*, Rev. Sci. Instrum. **82**, 113102 (2011).
[19] K.Y. Watanabe *et al.*, Plasma Phys. Control. Fusion **49**, 605 (2007).
[20] A. Kramida *et al.*, NIST Atomic Spectra Database (ver. 5.7.1), (2019). [Online]. Available: https://physics.nist.gov/asd [2020, October 27]. National Institute of Standards and Technology, Gaithersburg, MD. DOI: https://doi.org/10.18434/T4W30F
[21] R.L. Kelly, J. Phys. Chem. Ref. Data **16**, Suppl. 1 (1987).
[22] R. Katai *et al.*, Plasma Fusion Res. **2**, 014 (2007).
[23] X.L. Huang *et al.*, Rev. Sci. Instrum. **85**, 043511 (2014).
[24] C.F. Dong *et al.*, Rev. Sci. Instrum. **81**, 033107 (2010).
[25] E.H. Wang *et al.*, Rev. Sci. Instrum. **83**, 043503 (2012)
[26] H.M. Zhang *et al.*, Jpn. J. Appl. Phys. **54**, 086101 (2015).
[27] T. Oishi *et al.*, Appl. Opt. **53**, 6900 (2014).
[28] G. Kawamura *et al.*, Plasma Phys. Control. Fusion **60**, 084005 (2018).